THE JOURNAL OF PHYSICAL CHEMISTRY LETTERS
A JOURNAL OF THE AMERICAN CHEMICAL SOCIETY

pubs.acs.org/JPCL

Letter

The Q-Band Energetics and Relaxation of Chlorophylls *a* and *b* as Revealed by Visible-to-Near Infrared Time-Resolved Absorption Spectroscopy

Rong-Yao Gao,[⊥] Jian-Wei Zou,[⊥] Yan-Ping Shi, Dan-Hong Li, Junrong Zheng,* and Jian-Ping Zhang*

Cite This: *J. Phys. Chem. Lett.* 2025, 16, 789−794

Read Online

ACCESS | Metrics & More | Article Recommendations | Supporting Information

ABSTRACT: Chlorophyll (Chl) is the most abundant light-harvesting pigment of oxygenic photosynthetic organisms; however, the Q-band energetics and relaxation dynamics remain unclear. In this work, we have applied femtosecond time-resolved (*fs*-TA) absorption spectroscopy in 430−1,700 nm to Chls *a* and *b* in diluted pyridine solutions under selective optical excitation within their Q-bands. The results revealed distinct near-infrared absorption features of the $B_{x,y} \leftarrow Q_y$ and $B_{x,y} \leftarrow Q_x$ transitions in 930−1,700 nm, which together with the steady-state absorption in 400−700 nm unveiled the $Q_{x(0,0)}$-state energy that lies 1,000 ± 400 and 600 ± 400 cm^{-1} above the $Q_{y(0,0)}$-state for Chls *a* and *b*, respectively. In addition, the Q_x-to-Q_y internal conversion time constants are estimated to be less than 80 fs for Chls *a* and *b*. These findings may shed light on understanding the roles of the Chls in the primary excitation energy transfer reactions of photosynthesis.

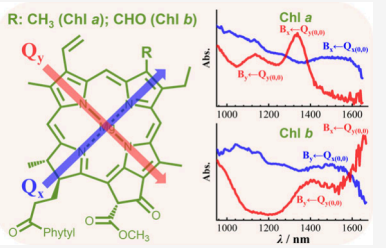

Chlorophyll (Chl) as an omnipresent photosynthetic pigment is essential for harvesting sunlight and commissioning the primary excitation energy transfer (EET) and charge separation (CS) reactions of oxygenic photosynthesis.[1] Some cyanobacteria and all green plants and algae are equipped with Chls, accounting for 17% of the photosynthetic membrane by weight.[2,3] Chls *a* and *b* intensely absorb light in blue (400−500) and red (600−700 nm) spectral regimes (Figure 1), and the respective absorption cross sections are referred to as the Soret (or B) and the Q bands following Gouterman's four-orbital model.[4] According to this theory, the Q_x (B_x) and Q_y (B_y) absorption stem from the transition dipole moments oriented along the diagonals, x and y, of the chlorin macrocycle (Figure S1a). Owing to the efficient internal conversion (IC) from the higher-lying singlet excited states, S_4 (B_y), S_3 (B_x) and S_2 (Q_x), to the lowest one, S_1 (Q_y), it is generally believed that the Q_y state play the essential role in conducting the EET and CS reactions in various Chl *a*/*b*-binding photosynthetic proteins, e. g., the light-harvesting antennae and the photoelectrochemical reaction centers (RCs).[5−9] Recent studies have suggested that the higher-lying states may also play a role in the primary EET reactions in pigment−protein complexes.[10−14]

For over half a century, the photophysics and photochemistry of Chls have received extensive experimental and theoretical research efforts.[14−25] However, only recently could the Q_x-state energy of Chl *a* be ascertained by using modern spectroscopic and quantum chemical means and could the mechanism of nonradiative relaxation of the Q_x-state be figured out. For example, recent investigations on Chl *a* in pyridine have shown that the Q_x state lies about 820 cm^{-1} (0.1 eV)

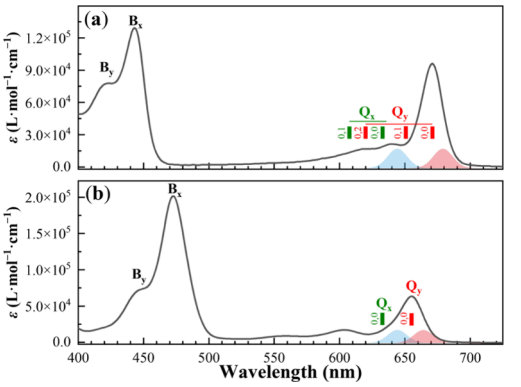

Figure 1. Ground-state absorption (GSA) spectra of (a) Chl *a* and (b) Chl *b* in pyridine solutions. Spectral origins of Q_x and Q_y vibronic bands are shown in red and green bars, respectively, and the associated numerals denote vibrational progression. Spectra of excitation pulses with a Gaussian line-shape are shown in blue (645 nm) or pink (680 or 665 nm), and the full width at half-maximum (fwhm) is 15 nm. Transition wavelengths of the vibronic bands of Chl *a* are from ref 26, and those of Chl *b* are determined in the present work.

Received: November 3, 2024
Revised: December 29, 2024
Accepted: January 9, 2025

https://doi.org/10.1021/acs.jpclett.4c03171
J. Phys. Chem. Lett. 2025, 16, 789−794

above the Q_y state.[26] Since the Q_x-Q_y energy separation is comparable to an energy quantum of molecular vibration (e. g., 700 cm^{-1}), the Q_x state may involve in the EET and/or CS reactions as a result of state mixing.[27,28] With regard to the mechanism of Q_x-to-Q_y IC, the conical intersection of potential energy surfaces (PESs)[25] and the vibronic coupling between these electronic states[28] have been proposed. Moreover, it was reported that, depending on the solvent, the IC process occurs with a time constant varying from 100 to 200 fs.[14,27,29] Despite the significant advances in understanding the energetics and the Q-band relaxation dynamic of Chl *a*, a paralleling understanding of Chl *b* has not been reached.

In terms of chemical structure, Chl *b* differs from Chl *a* merely by a formyl instead of a methyl group at C-7 (Figure S1a). The present work is intended to compare their Q-band energetics and nonradiative relaxation dynamics, with an emphasis on those of the Q_x state. To this end, we performed femtosecond time-resolved absorption (*fs*-TA) spectroscopy in 430−1,700 nm for Chls *a* and *b* in diluted pyridine solutions (10^{-5} M) with tuning the excitation wavelength in the Q-band. The *fs*-TA spectra in near-infrared region have divulged the distinct excited-state absorption (ESA) bands of $B_{x,y} \leftarrow Q_y$ transitions, and the broadband ESA features of $B_{x,y} \leftarrow Q_x$ transitions for both Chls, which allows the assessment of their Q-band energetics and relaxation dynamics.

Steady-State Absorption. Figure 1 shows the ground state absorption (GSA) spectra of Chls *a* and *b* in pyridine, a hexacoordination aprotic solvent. Chl *a* (Chl *b*) exhibits the characteristic B_x band at 443 nm (472 nm) and the $Q_{y(0,0)}$ band at 671 nm (655 nm). Compared to Chl *a*, Chl *b* has its B_x band red-shifted by 29 nm, and $Q_{y(0,0)}$ band blue-shifted by 16 nm, giving rise to a relatively narrower B-Q spectral gap. For Chl *a* in pyridine, previous anisotropic excitation spectroscopy, i.e. tracing the change in dichroic ratio of the infrared absorption of the keto C═O stretching mode (1,690 cm^{-1}) as a function of excitation wavelength, showed that the $Q_{x(0,0)}$ and $Q_{x(0,1)}$ bands locate at 636 and 607 nm, respectively, overlapping with the $Q_{y(0,1)}$ at 650 nm and the $Q_{y(0,2)}$ at 619 nm.[26] In addition, the $Q_{x(0,0)}$-$Q_{y(0,0)}$ energy separation of Chl *a* in pyridine is estimated to be 800−1,000 cm^{-1}, and the Q_x absorption contributes about 14−27% to the overall Q-band absorption in 590−720 nm.[14,26]

In the case of Chl *b*, the $Q_{y(0,0)}$ band peaks at 655 nm, and the stepwise of vibronic progression (spacing between vibronic bands, 1,320 and 1,530 cm^{-1}) is substantially larger than that of Chl *a* (720 and 610 cm^{-1}). However, the spectral origin of the $Q_{x(0,0)}$ band and its contribution to the overall Q-band absorption remain unclear. We have perceived via inspection of the GSA spectra that, given the $Q_{x(0,0)}$ location as depicted in Figure 1, the $B_{x,y} \leftarrow Q_{x(0,0)}$ transitions of Chls *a* and *b* would be readily detected by using near-infrared *fs*-TA spectroscopy. In this context, a recent theoretical work[28] predicted the $B_x \leftarrow Q_y$ ($B_y \leftarrow Q_y$) transition at 1,087 nm (940 nm), and the $B_x \leftarrow Q_x$ ($B_y \leftarrow Q_x$) transition at 1,396 nm (1,228 nm). In addition, for Chl *a* bound in the peridinin−chlorophyll-protein (PCP) complex, a $B \leftarrow Q_y$ ESA peaking around 1,290 nm was experimentally observed.[31]

Chl *a* Photoexcited at 680 nm. Figure 2a shows the transient spectra of Chl *a* within 3 ps after pulsed excitation at 680 nm. The asterisked peaks in the transients at 0.00 and 0.07 ps, which move systematically with varying excitation wavelength (λ_{exc}) (Figure 2, Figure S3), are originated from the stimulated Raman scattering of the solvent.[30] This assignment

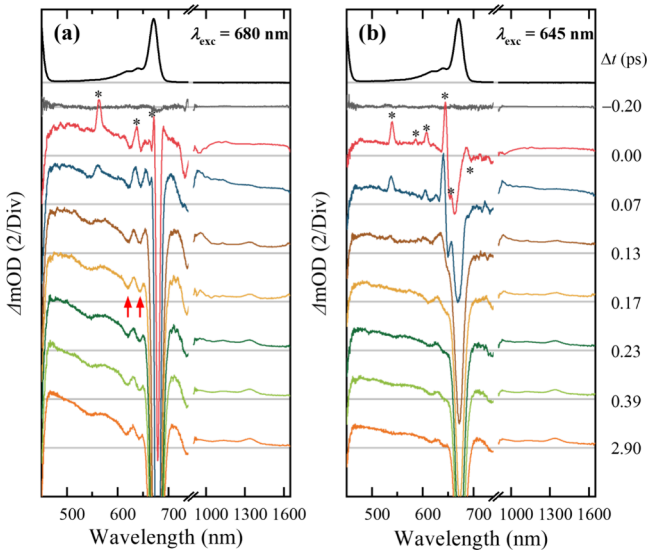

Figure 2. Visible-to-near-infrared *fs*-TA spectra at indicated delay time (Δt) for Chl *a* in pyridine under photoexcitation at (a) 680 nm and (b) 645 nm. For reference, the GSA spectrum of Chl *a* in pyridine is shown at the top of each panel. Asterisks indicate the stimulated Raman peaks of pyridine (see text for details). See Figure S2 for the spectra at later Δt decaying monotonically with a similar spectral pattern.

is confirmed by the nice agreement between the spectral distribution of the asterisked peaks and the stimulated Raman spectrum of neat pyridine (Figure S4a). Herein, we take the temporal profile of a Raman signal as the instrumental response function (i.r.f.) of our *fs*-TA spectrometer, and the according temporal width as the time resolution (80 fs, cf. Figure S4b).

The photoexcitation at 680 nm, in the red wing of the $Q_{y(0,0)}$ band peaking at 671 nm, in effect minimized the excess energy deposited in the Q_y state and the direct excitation of the Q_x state, which assures the intrinsic $Q_{y(0,0)}$ excitation dynamics to be examined. As seen in Figure 2a, at Δt > 0.13 ps, the non-negative dips in 600−650 nm (cf. upward arrows), residing on a broad ESA background, agree with the vibronic bands of the GSA spectrum. The intense negative band around 680 nm is the ground state bleaching (GSB) of $Q_{y(0,0)}$, which is accompanied by stimulated emission (SE) at longer wavelengths. Figures 3a plots the peak wavelength of this GSB band against delay time (Δt), and the trace at λ_{exc} = 680 nm shows systematic band shift toward *shorter*-wavelength side upon increasing Δt. The kinetics of this specific spectral shift could be well accounted for by a biexponential decay function, yielding the time constants as listed in Table 1. Since the pair of decay time constants are far shorter than the Q_y-state depopulation time (6.3 ns) as measured with time-resolved fluorescence spectroscopy (cf. Figure S5), the dynamic anti-Stokes shift reflects the processes of excitation equilibration in the Q_y state: Owing to the lack of excess energy, the slower process (τ_{d2} = 552 fs) can be attributed to vibrational redistribution among different vibrational modes rather than to the vibrational relaxation/cooling processes. Besides, the solvent redistribution around the excited molecule may modify its inhomogeneous environment, contributing to the blue shift of the 680 nm band. The faster process (τ_{d1} = 10 fs), not fully resolved with the present time resolution, is presumably ascribed to Q_x-Q_y electronic decoherence.[14,32] In this relation,

https://doi.org/10.1021/acs.jpclett.4c03171
J. Phys. Chem. Lett. 2025, 16, 789−794

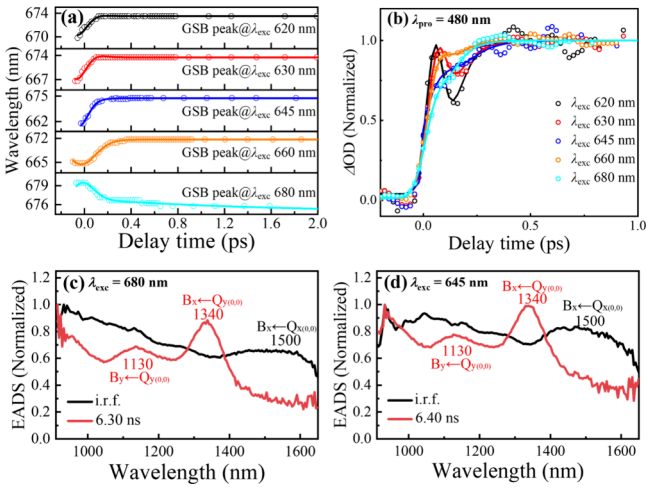

Figure 3. Kinetic traces in visible region and evolution associated difference spectra (EADSs) in near-infrared region for Chl *a* in pyridine. (a) Kinetic traces of dynamic spectral shift. (b) ESA kinetic traces at the probe wavelength (λ_{pro}) of 480 nm. Solid lines in panels (a) and (b) are fitting curves. (See Figure S3 for *fs*-TA spectra at λ_{exc} of 620, 630, and 660 nm.) (c, d) EADSs derived from the global analysis of *fs*-TA data sets in 930−1,700 nm recorded at the indicated λ_{exc}. The time constant of the i.r.f.-associated EADS is within i.r.f. (<10 fs).

Table 1. Decay and Rise Time Constants (τ_d, τ_r) of Chls *a* and *b* under Different Excitation Wavelengths (λ_{exc}) as Derived from the Kinetic Traces of Spectral Shift (Figures 3a, 5a) and ESA (Figures 3b, 5b) in Visible Region

		Dynamic shift		ESA kinetics	
Sample	λ_{exc} (nm)	τ_{d1} (fs)	τ_{d2} (fs)	τ_d (fs)	τ_r (fs)
Chl *a*	680	10 ± 1	552 ± 56	10 ± 1	62 ± 1
	660	13 ± 1	78 ± 6	28 ± 8	59 ± 4
	645	10 ± 2	73 ± 4	10 ± 1	80 ± 4
	630	12 ± 1	56 ± 14	11 ± 1	78 ± 2
	620	14 ± 1	77 ± 13	10 ± 1	99 ± 3
Chl *b*	665	11 ± 1	113 ± 27	11 ± 1	45 ± 2
	645	10 ± 1	148 ± 8	11 ± 1	42 ± 3
	630	9 ± 1	70 ± 3	11 ± 1	45 ± 2
	605	9 ± 1	62 ± 1	14 ± 6	56 ± 6

a 2-dimentional electronic spectroscopy (2DES) study of Chl *a* had revealed a 40 fs time scale of the electronic decoherence, which is proposed to be mediated via the coupling of a Q_y-vibrational mode with the Q_x state.[27]

It is seen from Figure 3b and Table 1 that, at λ_{exc} = 680 nm, the ESA kinetics probed at 480 nm rises monotonically with a time constant (τ_r) of 62 fs, whereas photoexcitation at a shorter λ_{exc} induced an additional decay component with a time constant (τ_d) of ∼10 fs. Caution must be taken for the assignment of the τ_d-component: It actually originates from the broad spectral background of the stimulated Raman scattering of pyridine (cf. Figure S4), i.e. irrelevant to Chl *a* excitation relaxation. Upon shortening λ_{exc} from 680 to 620 nm, the rise phase (τ_r) slows from ∼60 to ∼100 fs. In view of the direct Q_x photoexcitation at a shorter enough λ_{exc} (i.e., 645, 630, and 620 nm), the relatively slow rise can be related to the transfer of population from the Q_x to the Q_y state. The normalized ESA kinetics in Figure 3b exhibits apparent oscillation features. The first peak, which is more clearly discernible at a shorter λ_{exc}, originates from the ultrafast Raman response of pyridine, whereas the subsequent modulation seems at a noise level.

As seen in Figure 2a, in 930−1700 nm, distinct ESA features are observed around 950 nm (strong), 1,120 nm (weak), and 1,330 nm (strong). The global analysis based on singular value decomposition (SVD), although inapplicable to the visible *fs*-TA spectra owing to the forementioned dynamic spectral shift, can be applied to the near-infrared *fs*-TA data sets lacking of obvious spectral shift. Here, we note that, in the near-infrared region, the stimulated Raman process of neat pyridine also induced a short-lived, featureless spectral background (Figure S4a). In case the solvent and the Chl dynamics are temporally comparable, they can hardly be separated each other, which is unfortunately true herein. Nonetheless, we performed the global analysis of near-infrared *fs*-TA data sets based on a two-component sequential model.

Figure 3c shows the evolution associated difference spectra (EADSs) for the case of 680 nm excitation. The 6.3 ns-EADS (red curve) exhibits a pair of distinct bands peaking around 8,850 cm^{-1} (1,130 nm) and 7,463 cm^{-1} (1,340 nm), respectively, which agree well with the respective transition energies of $B_y \leftarrow Q_{y(0,0)}$ (8,794 cm^{-1}) and $B_x \leftarrow Q_{y(0,0)}$ (7,670 cm^{-1}) derived from the GSA spectrum (cf. Scheme 1). In addition, the ESA feature around 950 nm (10,526 cm^{-1}) can be assigned to the $S_n \leftarrow Q_{y(0,0)}$ transition with S_n representing higher-lying singlet excited states of Chl *a*. The i.r.f.-EADS (black curve), although could not be resolved temporally with the present resolution, involves an ultrafast ESA feature around 1,500 nm (6,667 cm^{-1}), which is entangled with the broad spectral background of neat pyridine (cf. Figure S4a). Assuming that this specific ESA is originated from the $Q_{x(0,0)}$ state, and taking into account the B_x-state energy (22,573 cm^{-1}, Scheme 1), we can locate the $Q_{x(0,0)}$ state at 629 ± 16 nm, which is in accord with that reported in ref 26 (636 nm). Here, we note that the rather broad ESA around 1,500 nm likely comprises two components at 1600 and 1400 nm with

Scheme 1. $B_{x,y}$ and $Q_{x,y}$ Energy Levels of Chls *a* and *b* along with $B_{x,y} \leftarrow Q_{y(0,0)}$ and $B_{x,y} \leftarrow Q_{x(0,0)}$ Transition Energies (Wavelengths)[a]

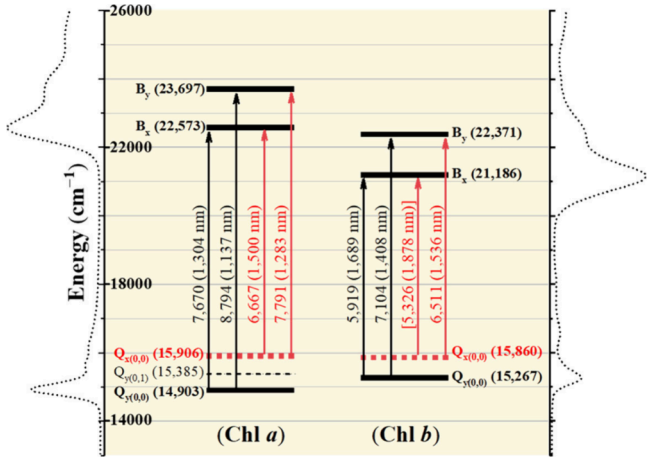

[a]Vertical arrows represent the electronic transitions. The transition energies in black font are derived from GSA spectra (shown in dotted line for reference), and those in red font are estimated on the basis of near-infrared EADSs (see text for details). The energy level of Chl *a* $Q_{y(0,1)}$ is from ref 26, and the energetic order of Chl *a* $B_{x,y}$ is as that assigned in refs 34, 35.

https://doi.org/10.1021/acs.jpclett.4c03171
J. Phys. Chem. Lett. 2025, 16, 789−794

respective energetic separation of 530 and 1,420 cm^{-1} from $Q_{y(0,0)}$. These components are in accord with the pair of $Q_{x(0,0)}$ bands lying 620 and 1,640 cm^{-1} above the $Q_{y(0,0)}$ band as observed for Chl *a* in pyridine with magnetic circular dichroism (MCD), which are explained in terms of $Q_{x(0,0)}$-$Q_{y(0,1)}$ vibronic coupling.[14,36] Accordingly, the excitation light with a spectral bandwidth of 15 nm (fwhm) inevitably excited the $Q_{y(0,1)}$ state and hence the coupled $Q_{x(0,0)}$ state because of the vibronic coupling.

Chl *a* Photoexcited at 645 nm. In view of the congestion of Q-band vibrational levels, photoexcitation of Chl *a* at 645 nm is expected to populate the $Q_{y(0,1)}$ and $Q_{x(0,0)}$ states with equal partition. The *fs*-TA spectra in Figure 2b are seemingly similar to those under 680 nm excitation, however, the major GSB peak shifts to longer- instead of shorter-wavelength side upon 680 nm excitation, and the τ_{d2} at λ_{exc} = 645 nm becomes much shorter (73 fs vs 552 fs; Figure 3a, Table 1). It is interesting to see that despite the involvement of the $Q_{x(0,0)}$ state upon 645 nm excitation, the near-infrared ESAs are similar to those upon 680 nm excitation, which consolidates the aforementioned assignments of near-infrared transitions. Note that the $B_x \leftarrow Q_{x(0,0)}$ transition at ~1,500 nm was observed even under 680 nm excitation (without directly targeting the $Q_{x(0,0)}$ state). Such λ_{exc}-independence of EADS further supports the presence of $Q_{x(0,0)}$-$Q_{y(0,1)}$ coupling, as proposed above.

Chl *b* Photoexcited at 665 and 645 nm. Figure 4a shows the representative *fs*-TA spectra in 3 ps recorded for Chl *b* photoexcited at 665 nm, the red edge of the $Q_{y(0,0)}$ band. In 450−650 nm, the GSB of the Soret band appears at 471 nm. The non-negative dips around 550 and 600 nm (cf. upward arrows) agree well with the vibronic bands of the inverted GSA spectrum. In 930−1700 nm, distinct ESA features are seen around 940 nm (stronger) and 1,400 and 1,650 nm (weaker).

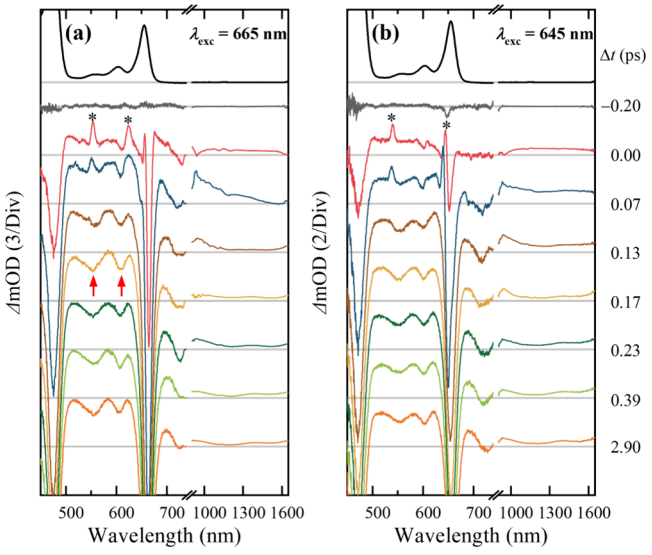

Figure 4. Visible-to-near-infrared *fs*-TA spectra at indicated delay time (Δt) for Chl *b* in pyridine photoexcited at (a) 665 nm and (b) 645 nm. For reference, the GSA spectrum of Chl *b* in pyridine is shown at the top of each panel. Asterisks indicate the stimulated Raman peaks of pyridine (*vide supra*). See Figure S6 for the spectra at later Δt decaying monotonically with a similar spectral pattern.

Figure 5a shows the kinetic traces in 2 ps for the dynamic spectral shift of the major Q_y GSB band. Similar to the cases of

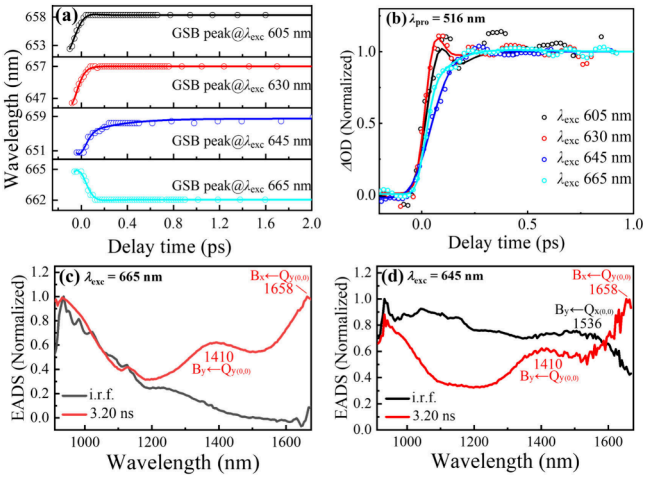

Figure 5. Kinetic traces in visible region and EADSs in near-infrared region for Chl *b* in pyridine. (a) Kinetic traces of dynamic spectral shift. (b) ESA kinetic traces at λ_{pro} = 516 nm. Solid lines in panels (a) and (b) are fitting curves. (See Figure S7 for *fs*-TA spectra at λ_{exc} of 605 and 630 nm.) (c, d) EADSs derived from the global analysis of *fs*-TA data sets in 930−1,700 nm recorded at the indicated λ_{exc}. The time constant of the i.r.f.-associated EADS is within i.r.f. (<10 fs).

Chl *a*, curve fitting of these kinetic traces yielded a pair of decay time constants as listed in Table 1. Under λ_{exc} = 665 nm, the dynamic blue shift reflects the excitation equilibration in the Q_y state. Photoexcitation of Chl *b* at 665 and 645 nm resulted in similar τ_{d2} time constants of 113 and 148 fs, respectively, indicating that the Q_y-state vibrational redistribution of Chl *b* is significantly faster than that of Chl *a* (552 fs). In addition, a similar τ_{d2} upon the blue- and red-edge excitation implies the lack of any principal vibrational level between the $Q_{x(0,0)}$ and the $Q_{y(0,0)}$ state (Scheme 1). In this relation, the GSA spectrum of Chl *b* exhibits considerably larger stepwise vibrational progression than that of Chl *a*, implying the different alignments of their vibrational levels. On the other hand, in view of the lack of excess energy, the τ_{d1} components can be putatively attributed to the Q_x-Q_y decoherence (*vide supra*). Interestingly, shortening λ_{exc} to 630 nm and further to 605 nm, i.e. with increase of excess energy, the τ_{d2}-component decay is twice accelerated (60−70 fs) with respect to the cases of 665 and 645 nm excitation (110−150 fs), which is indicative of the involvement of electronic relaxation.

As seen from Figure 5b and Table 1, the ESA kinetics at a λ_{exc} of 665 nm rises monotonically with a time constant (τ_r) of 45 fs. Shortening the λ_{exc} leads to an additional fast decay component with ($\tau_d \sim 10$ fs), whereas the rise component (τ_r) remains essentially unvaried. Notably, the overall electronic relaxation among the manifold of $Q_{x,y}$ state (40−60 fs) is significantly faster than that of Chl *a* (60−100 fs), cf. Table 1. As in the case of Chl *a*, the τ_d-component is contributed mainly by the ultrafast Raman response of pyridine (cf. Figure S4), irrelevant to the Chl *b* dynamics.

In Figure 5c, the 3.2 ns-EADS shows distinct $B_y \leftarrow Q_{y(0,0)}$ and $B_x \leftarrow Q_{y(0,0)}$ absorption features peaking around 1,410 and 1,658 nm, respectively. The spectral assignments are based on the fact that the respective transition energies (7,092 and 6,031 cm^{-1}) agree nicely with those derived from the GSA spectrum (7,104 and 5,919 cm^{-1}), cf. Scheme 1. Importantly, the other EADS in Figure 5c resembles intimately the spectral

https://doi.org/10.1021/acs.jpclett.4c03171
J. Phys. Chem. Lett. 2025, 16, 789−794

background of pure pyridine (cf. Figure S4a), implying that photoexcitation of Chl *b* at 665 nm avoided direct excitation of the Q_x state. In this relation, the MCD spectra of Chl *b* in nematic liquid crystal metrices exhibit a single $Q_{x(0,0)}$ band,[37] indicating the lack of $Q_{x(0,0)}$-$Q_{y(0,1)}$ vibronic coupling as found for Chl *a* (*vide supra*).[14] On the other hand, for Chl *b* photoexcited at 645 nm (Figure 5d), the i.r.f.-associated EADS entangling with the solvent background exhibits an ESA band around 1,536 nm due to the concurrent excitation of Q_x and Q_y. This broadband feature can be ascribed to the $B_y \leftarrow Q_{x(0,0)}$ rather than the $B_x \leftarrow Q_{x(0,0)}$ transition, because the spectral origin of $Q_{x(0,0)}$ would otherwise appear around 681 nm (i.e., to the red side of the $Q_{y(0,0)}$ band), which is obviously unreasonable. As such, the spectral origin of Chl *b* $Q_{x(0,0)}$ can be placed at 631 ± 16 nm as estimated by subtracting the transition energy at 1,536 nm from the B_y-state energy (Scheme 1). Accordingly, the $B_x \leftarrow Q_{x(0,0)}$ transition may appear around 1,878 nm, which is out of the present spectral window. At the moment, it is not feasible to locate the higher-lying vibrational levels of Chl *b*. To the best of our knowledge, the $Q_{x(0,0)}$ state energy of Chl *b* has not been reported hitherto. Nevertheless, it is surprising for us to see that Chls *a* and *b* share a similar $Q_{x(0,0)}$ energy, and that the $Q_{x(0,0)}$-$Q_{y(0,0)}$ energy gap of Chl *b* is as small as 600 cm^{-1} (Scheme 1).

Finally, we consider the Q_x-to-Q_y IC process. The IC time constants for Chls *a* and *b*, respectively, had been reported to be 100−200 fs and 150−250 fs depending on solvent.[13,26] Herein, it is noteworthy that the ultrafast solvent response must be taken into account in interpreting the ultrafast time-resolved spectra of diluted Chl solutions. In addition, recent 2DES studies of Chl *a* solution with coherent excitation of Q_x and Q_y vibronic bands had revealed an overall Q_x-to-Q_y IC time constant of 170 fs.[27,33] The present work succeeded in detecting the Q_x-state ESA in the near-infrared region. However, with a time resolution of 80 fs we could not resolve the Q_x-to-Q_y IC time scales, implying considerably faster IC processes of Chls *a* and *b* than those reported previously.

In Summary, we have observed characteristic $B_y \leftarrow Q_{y(0,0)}$, $B_x \leftarrow Q_{y(0,0)}$ and $B_x \leftarrow Q_{x(0,0)}$ ESAs of Chl *a* at 1,130, 1,340 and 1,500 nm, respectively, as well as the $B_y \leftarrow Q_{y(0,0)}$, $B_x \leftarrow Q_{y(0,0)}$ and $B_y \leftarrow Q_{x(0,0)}$ ESAs of Chl *b* at 1,410, 1,658 and 1,536 nm, respectively. The characteristic ESAs combined with the GSA spectra allows us to determine the $Q_{x(0,0)}$-state energies, which turn out to be similar between Chl *a* (15,906 cm^{-1}) and Chl *b* (15,860 cm^{-1}). Accordingly, the $Q_{x(0,0)}$-$Q_{y(0,0)}$ energy gaps are found to be ∼1,000 and ∼600 cm^{-1} for Chls *a* and *b*, respectively. In addition, based on the spectral evolution dynamics in visible and near-infrared regions, we conclude that the Q_x-to-Q_y IC time scales of Chls *a* and *b* are most likely less than 80 fs. These findings will be of help for interpreting the spectral dynamics of Chl *a*/*b* binding proteins and may shed light on understanding the light-conversion mechanisms of natural and artificial photosynthetic systems.

■ ASSOCIATED CONTENT

Supporting Information

The Supporting Information is available free of charge at https://pubs.acs.org/doi/10.1021/acs.jpclett.4c03171.

Chls *a* and *b* structures and purity check, and additional *fs*-TA spectra and kinetic traces (PDF)

Transparent Peer Review report available (PDF)

■ AUTHOR INFORMATION

Corresponding Authors

Junrong Zheng − *College of Chemistry and Molecular Engineering, Beijing National Laboratory for Molecular Sciences, Peking University, Beijing 100871, China;* orcid.org/0000-0002-4472-8576; Email: junrong@pku.edu.cn

Jian-Ping Zhang − *Key Laboratory of Advanced Light Conversion Materials and Biophotonics, School of Chemistry and Life Resources, Renmin University of China, Beijing 100872, P. R. China;* orcid.org/0000-0002-9216-2386; Email: jpzhang@ruc.edu.cn

Authors

Rong-Yao Gao − *Key Laboratory of Advanced Light Conversion Materials and Biophotonics, School of Chemistry and Life Resources, Renmin University of China, Beijing 100872, P. R. China*

Jian-Wei Zou − *College of Chemistry and Molecular Engineering, Beijing National Laboratory for Molecular Sciences, Peking University, Beijing 100871, China*

Yan-Ping Shi − *Key Laboratory of Advanced Light Conversion Materials and Biophotonics, School of Chemistry and Life Resources, Renmin University of China, Beijing 100872, P. R. China*

Dan-Hong Li − *Key Laboratory of Advanced Light Conversion Materials and Biophotonics, School of Chemistry and Life Resources, Renmin University of China, Beijing 100872, P. R. China;* Present Address: Department of Biochemistry, School of Biological and Behavioral Sciences, Queen Mary University of London, London E1 4NS, United Kingdom

Complete contact information is available at: https://pubs.acs.org/10.1021/acs.jpclett.4c03171

Author Contributions

⊥J.-W. Z. and R.-Y. G. contributed equally to this work. J.-W. Z. conducted *fs*-TA experiment. Y.-P. S. and R.-Y. G. prepared samples. J.-P. Z., R.-Y. G., D. L. and J. Z. jointly wrote the manuscript, and all authors contributed to data analysis, result discussion and manuscript revision.

Notes

The authors declare no competing financial interest.

■ ACKNOWLEDGMENTS

This project has been supported by the Natural Science Foundation of China (NSFC, Nos. 22173115; 92261206; 21927901).

■ REFERENCES

(1) Croce, R.; van Amerongen, H. Light harvesting in oxygenic photosynthesis: structural biology meets spectroscopy. *Science* **2020**, *369*, 6506.

(2) Koochak, H.; Puthiyaveetil, S.; Mullendore, D. L.; Li, M.; Kirchhoff, H. The structural and functional domains of plant thylakoid membranes. *Plant J.* **2019**, *97*, 412−429.

(3) Croce, R.; van Amerongen, H. Natural strategies for photosynthetic light harvesting. *Nat. Chem. Biol.* **2014**, *10*, 492−501.

(4) Gouterman, M. Spectra of porphyrins. *J. Mol. Spectrosc.* **1961**, *6*, 138−163.

(5) Zheng, M.; Zhou, C.; Wang, W.; Kuang, T.; Shen, J.; Tian, L. Origin of energy dissipation in the oligomeric fucoxanthin-chlorophyll *a*/*c* binding proteins. *J. Phys. Chem. Lett.* **2023**, *14*, 7967−7974.

(6) Wells, K. L.; Lambrev, P. H.; Zhang, Z.; Garab, G.; Tan, H.-S. Pathways of energy transfer in LHCII revealed by room-temperature 2D electronic spectroscopy. *Phys. Chem. Chem. Phys.* **2014**, *16*, 11640−11646.
(7) Zhang, Z.; Lambrev, P. H.; Wells, K. L.; Garab, G.; Tan, H.-S. Direct observation of multistep energy transfer in LHCII with fifth-order 3D electronic spectroscopy. *Nat. Commum.* **2015**, *6*, 7914.
(8) Renger, G.; Renger, T. Photosystem II: the machinery of photosynthetic water splitting. *Photosynth. Res.* **2008**, *98*, 53−80.
(9) Mamedov, M.; Govindjee; Nadtochenko, V.; Semenov, A. Primary electron transfer processes in photosynthetic reaction centers from oxygenic organisms. *Photosynth. Res.* **2015**, *125*, 51−63.
(10) Götze, J. P.; Lokstein, H. Excitation energy transfer between higher excited states of photosynthetic pigments: 1. carotenoids intercept and remove B band excitations. *ACS Omega* **2023**, *8*, 40005−40014.
(11) Götze, J. P.; Lokstein, H. Excitation energy transfer between higher excited states of photosynthetic pigments: 2. chlorophyll *b* is a B band excitation trap. *ACS Omega* **2023**, *8*, 40015−40023.
(12) Götze, J. P.; Kröner, D.; Banerjee, S.; Karasulu, B.; Thiel, W. Carotenoids as a shortcut for chlorophyll Soret-to-Q band energy flow. *ChemPhysChem* **2014**, *15*, 3392−3401.
(13) Bricker, W. P.; Shenai, P. M.; Ghosh, A.; Liu, Z.; Enriquez, M. G. M.; Lambrev, P. H.; Tan, H.-S.; Lo, C. S.; Tretiak, S.; Fernandez-Alberti, S.; Zhao, Y. Non-radiative relaxation of photoexcited chlorophylls: theoretical and experimental study. *Sci. Rep.* **2015**, *5*, 13625.
(14) Reimers, J. R.; Cai, Z.-L.; Kobayashi, R.; Rätsep, M.; Freiberg, A.; Krausz, E. Assignment of the Q-bands of the chlorophylls: coherence loss via Q_x-Q_y mixing. *Sci. Rep.* **2013**, *3*, 2761.
(15) Seely, G. R. The energetics of electron-transfer reactions of chlorophyll and other compounds. *Photochem. Photobiol.* **1978**, *27*, 639−654.
(16) Dahlbom, M. G.; Reimers, J. R. Successes and failures of time-dependent density functional theory for the low-lying excited states of chlorophylls. *Mol. Phys.* **2005**, *103*, 1057−1065.
(17) Niedzwiedzki, D. M.; Blankenship, R. E. Singlet and triplet excited state properties of natural chlorophylls and bacteriochlorophylls. *Photosynth. Res.* **2010**, *106*, 227−238.
(18) Renge, I.; Mauring, K. Spectral shift mechanisms of chlorophylls in liquids and proteins. *Spectrochim. Acta Part A* **2013**, *102*, 301−313.
(19) Shenai, P. M.; Fernandez-Alberti, S.; Bricker, W. P.; Tretiak, S.; Zhao, Y. Internal conversion and vibrational energy redistribution in chlorophyll A. *J. Phys. Chem. B* **2016**, *120*, 49−58.
(20) Krüger, T. P. J.; van Grondelle, R. The role of energy losses in photosynthetic light harvesting. *J. Phys. B: At. Mol. Opt. Phys.* **2017**, *50*, 132001.
(21) Kosumi, D.; Nishiguchi, T.; Amao, Y.; Cogdell, R. J.; Hashimoto, H. Singlet and triplet excited states dynamics of photosynthetic pigment chlorophyll *a* investigated by sub-nanosecond pump-probe spectroscopy. *J. Photochem. Photobiol. A: Chem.* **2018**, *358*, 374−378.
(22) Song, Y.; Schubert, A.; Maret, E.; Burdick, R. K.; Dunietz, B. D.; Geva, E.; Ogilvie, J. P. Vibronic structure of photosynthetic pigments probed by polarized two-dimensional electronic spectroscopy and *ab initio* calculations. *Chem. Sci.* **2019**, *10*, 8143−8153.
(23) Sirohiwal, A.; Berraud-Pache, R.; Neese, F.; Izsák, R.; Pantazis, D. A. Accurate computation of the absorption spectrum of chlorophyll *a* with pair natural orbital coupled cluster methods. *J. Phys. Chem. B* **2020**, *124*, 8761−8771.
(24) Fortino, M.; Collini, E.; Bloino, J.; Pedone, A. Unraveling the internal conversion process within the Q-bands of a chlorophyll-like-system through surface-hopping molecular dynamics simulations. *J. Chem. Phys.* **2021**, *154*, 094110.
(25) Liu, H.; Ruan, M.; Mao, P.; Wang, Z.; Chen, H.; Weng, Y. Unraveling the excited-state vibrational cooling dynamics of chlorophyll-*a* using femtosecond broadband fluorescence spectroscopy. *J. Chem. Phys.* **2024**, *160*, 205101.
(26) Zahn, C.; Stensitzki, T.; Heyne, K. Femtosecond anisotropy excitation spectroscopy to disentangle the Q_x and Q_y absorption in chlorophyll *a*. *Chem. Sci.* **2022**, *13*, 12426−12432.
(27) Meneghin, E.; Leonardo, C.; Volpato, A.; Bolzonello, L.; Collini, E. Mechanistic insight into internal conversion process within Q-bands of chlorophyll *a*. *Sci. Rep.* **2017**, *7*, 11389.
(28) Reiter, S.; Bäuml, L.; Hauer, J.; de Vivie-Riedle, R. Q-band relaxation in chlorophyll: new insights from multireference quantum dynamics. *Phys. Chem. Chem. Phys.* **2022**, *24*, 27212−27223.
(29) Shi, Y.; Liu, J. Y.; Han, K. L. Investigation of the internal conversion time of the chlorophyll *a* from S_3, S_2 to S_1. *Chem. Phys. Lett.* **2005**, *410*, 260−263.
(30) Dhamija, S.; Bhutani, G.; Jayachandran, A.; De, A. K. A revisit on impulsive stimulated Raman spectroscopy: importance of spectral dispersion of chirped broadband probe. *J. Phys. Chem. A* **2022**, *126*, 1019−1032.
(31) Zigmantas, D.; Hiller, R. G.; Sundström, V.; Polívka, T. Carotenoid to chlorophyll energy transfer in the peridinin-chlorophyll *a* protein complex involves an intramolecular charge transfer state. *Proc. Natl. Acad. Sci. U. S. A.* **2002**, *99*, 16760−16765.
(32) Seibt, J.; Lindorfer, D.; Renger, T. Signatures of intramolecular vibrational and vibronic Q_x-Q_y coupling effects in absorption and CD spectra of chlorophyll dimers. *Photosynth. Res.* **2023**, *156*, 19−37.
(33) Moca, R.; Meech, S. R.; Heisler, I. A. Two-dimensional electronic spectroscopy of chlorophyll *a*: solvent dependent spectral evolution. *J. Phys. Chem. B* **2015**, *119*, 8623−8630.
(34) Thomas, L. L.; Kim, J. H.; Cotton, T. M. Comparative study of resonance Raman and surface-enhanced resonance Raman chlorophyll *a* spectra using Soret and red excitation. *J. Am. Chem. Soc.* **1990**, *112*, 9378−9386.
(35) Weiss, C. The pi electron absorption spectra of chlorophylls in solution. *J. Mol. Spectrosc.* **1972**, *44*, 37−80.
(36) Reimers, J. R.; Rätsep, M.; Freiberg, A. Asymmetry in the Q_y fluorescence and absorption spectra of chlorophyll *a* pertaining to exciton dynamics. *Front. Chem.* **2020**, *8*, 588289.
(37) Frackowiak, D.; Bauman, D.; Manikowski, H.; Browett, W. R.; Stillman, M. J. Circular dichroism and magnetic circular dichroism spectra of chlorophylls *a* and *b* in nematic liquid crystals. *Biophys. Chem.* **1987**, *28*, 101−104.

https://doi.org/10.1021/acs.jpclett.4c03171
J. Phys. Chem. Lett. 2025, 16, 789−794